An ultraslow-spreading class of ocean ridge

Henry J. B. Dick, Jian Lin & Hans Schouten

Woods Hole Oceanographic Institution, Woods Hole, Massachusetts 02543, USA

New investigations of the Southwest Indian and Arctic ridges reveal an ultraslow-spreading class of ocean ridge that is characterized by intermittent volcanism and a lack of transform faults. We find that the mantle beneath such ridges is emplaced continuously to the seafloor over large regions. The differences between ultraslow- and slow-spreading ridges are as great as those between slow- and fast-spreading ridges. The ultraslow-spreading ridges usually form at full spreading rates less than about 12 mm yr^{-1}, though their characteristics are commonly found at rates up to approximately 20 mm yr^{-1}. The ultraslow-spreading ridges consist of linked magmatic and amagmatic accretionary ridge segments. The amagmatic segments are a previously unrecognized class of accretionary plate boundary structure and can assume any orientation, with angles relative to the spreading direction ranging from orthogonal to acute. These amagmatic segments sometimes coexist with magmatic ridge segments for millions of years to form stable plate boundaries, or may displace or be displaced by transforms and magmatic ridge segments as spreading rate, mantle thermal structure and ridge geometry change.

Ocean ridges spreading at less than ~20 mm yr^{-1} comprise ~20,000 km of the ~55,000 km global ridge system[1], but until recently have been little studied. On the basis of studies at faster spreading rates, ocean ridges have been divided into fast-, intermediate-, and slow-spreading, each with distinctive morphologic characteristics (Fig. 1a). Slow-spreading ridges (less than ~55 mm yr^{-1}) have deep rift valleys with highly variable relief from ~400 to 2,500 m (ref. 2) and rough rift mountain topography weakly correlated to spreading rate[3]. Fast-spreading ridges (~80–180 mm yr^{-1}) have low (~400 m) axial highs[4], sometimes with small linear depressions (less than ~100 m wide and less than ~10 m deep, for example[5]) at their crests, and minimal rift mountain topography uncorrelated to spreading rate. Intermediate-spreading ridges (~55–70 mm yr^{-1}; ref. 2) have long alternating sections with either slow- or fast-spreading ridge morphology[6–8].

Slow-spreading ridges near mantle hotspots that have an axial rise (for example, the Reykjanes ridge), and abrupt changes in morphology at intermediate-spreading-rate ridges, show that ridge morphology is not strictly dependent on spreading rate, but may reflect variations in ridge geometry, melt supply, and mantle composition and thermal structure.

But this classification also does not take into account variations in crustal thickness with spreading rate. Although seismic crustal thickness shows little dependency on spreading rate down to 20 mm yr^{-1}, it then drops off rapidly (Fig. 1b). Models for buoyant and passive plate-driven mantle flow attribute this to conductive cooling from above depressing the top of the mantle melting column and limiting melt production[9–12]. Thus, changes in ridge geometry, mantle composition, flow and thermal structure that at faster rates would have a minor effect, dramatically affect crustal production and tectonics at very slow spreading rates[13,14], creating a class of ridges that is distinct from previous categories.

Just as the East Pacific Rise is the only fast-spreading ridge, the only ultraslow-spreading ridge is the Gakkel ridge in the Arctic Ocean: an 1,800-km-long ridge without transform faults spreading 8 to 13 mm yr^{-1} (ref. 15). The very-slow-spreading (14–16 mm yr^{-1}) Southwest Indian ridge (SWIR) and the remaining Arctic ridge system (13–18 mm yr^{-1}) are transitional between slow and ultraslow. Just as intermediate-rate ridges alternate between fast and slow morphology, these ridges alternately exhibit slow or ultraslow ridge characteristics over long sections. Thus, there are two intermediate-ridge classes rather than one, representing transitions from fast- to slow-spreading and slow- to ultraslow-spreading tectonics (Fig. 1b).

Magmatic accretionary ridge segments are second-order segments that link together between transform faults to make up first-order segments[16]. They are considered the basic unit of magmatic accretion, and at slow-spreading ridges often have circular negative mantle Bouguer anomalies (MBAs) centred on them, suggesting focused melt and/or mantle flow resulting in thicker crust at their centres[17–20]. As there are no transform faults defining a first-order segmentation at ultraslow rates, we use the term 'supersegment' to describe distinct physiographic regions consisting of linked magmatic and amagmatic ridge segments.

Magmatic segments form sub-perpendicularly to the least principal compressive stress, at an angle intermediate to the ridge trend and orthogonal to the spreading direction, for example[21,22]. Morphologically, they consist of linear axial highs or troughs with saddle points at the segment centres and rift valley walls consisting of staircase normal boundary faults. In the absence of transform faults, these structures occur in sets overlapping en echelon or connect by small non-transform discontinuities to accommodate plate boundary trends that are oblique to the spreading direction. Where the ridge trend is highly oblique (for example, the Mohns ridge), intrarift faults and axial ridges often have sigmoidal traces where they merge with rift valley bounding faults that run at higher angles subparallel to the ridge trend[21]. The close interaction of these two fault sets shows that they are part of an integrated system accommodating oblique extension during brittle faulting in the shallow crust (for example, ref. 22).

Amagmatic accretionary ridge segments are a key component of ultraslow-spreading ridges, replacing transform faults while extending the zone of lithospheric accretion. In contrast to magmatic segments, they assume any orientation relative to the spreading direction, and are usually marked by an axial trough rarely more than a kilometre deep that may extend 50 km or more. They have only scattered volcanics or a thin basalt carapace, virtually no seismic layer 3 (for example, ref. 23), expose abundant mantle peridotite, and have weak magnetization and a relatively positive MBA. The basic accretion unit appears to be mantle horst blocks rising up through the rift valley floor along an axis running parallel to the plate boundary trend. These are subsequently uplifted to create the axial trough walls—often creating single ~14°–20° low-angle fault surfaces bounding lenticular peridotite ridges.

The SWIR from 9° to 25° E

The SWIR has a very oblique trend—typically ~60° from the spreading direction—and is an example of a transitional ridge between slow and ultraslow. Long sections are similar to slow-spreading ocean ridges (that is, second-order magmatic segments linked by transform faults). Other sections lack transforms and have the character of ultraslow ridges, consisting of sub-orthogonal ~50-km-long magmatic segments linked by amagmatic oblique troughs (for example, ref. 24). This slow to ultraslow transitional behaviour is probably largely due to the influence of ridge geometry. As obliquity increases ridge length, mantle upwelling rate must slow proportionately (Fig. 2b, inset). This is expressed by the spreading component perpendicular to the ridge trend: the effective spreading rate for mantle upwelling (ESR). At very slow spreading rates less than ~20 mm yr^{-1}, varying ESR (and mantle composition and temperature) creates a region in the spreading-rate spectrum where ridges can assume either a slow-spreading or an ultraslow-spreading morphology.

The two sharply contrasting supersegments along the 1,000 km of the SWIR between the Shaka fracture zone at 9° E and the Prince Edward fracture zone at 25° E, provides a case in point (Fig. 2). The eastern 'orthogonal' supersegment, mapped in ref. 25, extends 600 km from 16° to 25° E and has 330- and 191-km-long subsections oriented approximately perpendicularly to the spreading direction linked by a 150-km slightly oblique (~10°) section (Fig. 2b). From 17° E, the ridge curves smoothly to the southwest, and thus the ESR steadily decreases to the west. At 16° E there is an abrupt change in ridge morphology and lithology at an ESR of ~12 mm yr^{-1}. Further west the ridge reaches an obliquity of 32° from the spreading direction, resulting in possibly the lowest ESR on the global ridge system (7.8 mm yr^{-1}). This continuous change in ESR without a major ridge offset provided an opportunity to examine the influence of mantle upwelling on crustal accretion at the slowest end of the spreading spectrum. Thus, in austral summer 2000, during RV *Knorr* Cruise 162, we mapped gravity, magnetics and bathymetry along the 'oblique supersegment' out to ~10–11 Myr ago or ~85 km from the ridge axis on a flow line, extensively sampling both supersegments.

The orthogonal supersegment is morphologically and geophysically similar to first-order ridge segments along the slow-spreading Mid-Atlantic Ridge[25] (MAR) (Fig. 2 legend). To complement 13 previous dredges, we made 28 more along the orthogonal supersegment (Fig. 2a): providing 26 along the axis and 15 on the rift valley walls. Dredge tracks were typically 500 m or more in length. Nine were empty, whereas 30 contained glassy pillow basalt. Gabbro and peridotite occur in only one wall dredge, consistent with the seafloor physiography, which suggested a nearly continuous volcanic carapace.

The oblique supersegment begins at the 16° E discontinuity with a 500-m drop in rift valley depth (Fig. 2a) and abrupt changes in physiography, MBA, magnetic anomaly intensity, and rocks dredged (Fig. 3). Although the spreading appears well organized, the pattern and tectonic character of the supersegment is very unlike that of 16°–25° E, consisting of linked magmatic and amagmatic accretionary ridge segments.

The westernmost region from 9° 30′ to 11° 45′ E is a broad area of rough topography with a short magmatic ridge segment at its intersection with the Shaka fracture zone. From there, a poorly defined rift valley and an irregular terrain run obliquely to the northeast to abut the west flank of Joseph Mayes seamount. This seamount is the first of only two significant volcanic centres on the supersegment. It splits an old lineated peridotite block that projects from its northeastern and southwestern flanks on an axis perpendicular to the spreading direction, filling the rift valley to create a 2,500-m high double-peaked volcano. Five dredges on the volcano recovered fresh pillow basalt.

East of Mayes seamount, there is a 180-km-long, 4,200-m-deep oblique amagmatic segment from 11° 30′ to 14° 24′ E, oriented 32° from the spreading direction. It has an axial trough with local deep areas to 4,700 m. Twenty-two dredges (2,574 kg) recovered 46.2% serpentinized peridotites, 2.6% dunite, 14.2% pillow basalt, 19.9% basalt and diabase, and 12.6% hydrothermal silica, sepiolite, and massive sulphides from the trough walls and floor. As even a thin basalt flow effectively covers peridotite emplaced to the seafloor, the dredge statistics and lack of gabbro show that igneous crust is thin or absent here and that the terrain is largely created by faulting. Although the trough floor is rough, with ~500-m relief, there is no morphologic evidence of a neovolcanic zone. Rather, long irregular axial horst blocks rise up from the valley floor. Dredging, physiography, weak magnetization, and positive MBA suggest these blocks

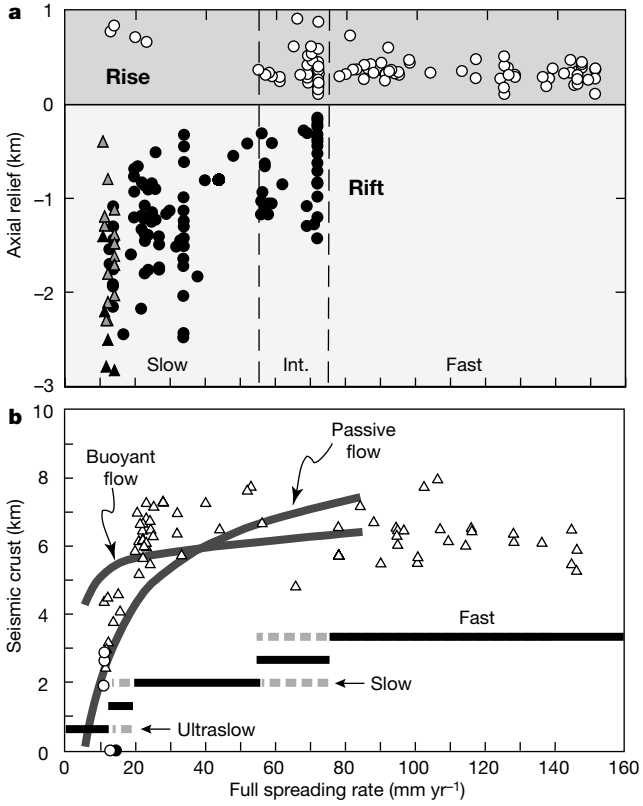

Figure 1 Ridge properties as a function of spreading rate. **a**, Axial relief versus spreading rate. Axial rises shown by white circles and axial rifts by black circles modified from ref. 2. Triangles show new Gakkel ridge[15] and SWIR 9°–16° E data: grey triangles, amagmatic accretionary segments; black triangles, magmatic ridge segments. Note that the amagmatic segments have lower relief. Dashed lines show a conventional division for ocean ridges into fast-, intermediate- (Int.) and slow-spreading with intermediate-spreading ridges those consistently exhibiting alternate fast and slow behaviour. **b**, Seismic crustal thickness versus spreading rate from ref. 12 (white triangles). White circles are new Gakkel ridge values (AMORE)[23]; black filled circle is for SWIR 9°–16° E oblique supersegment. Zero values are based on dredging. Crustal thickness curves calculated for passive flow[48] and buoyant flow[49] models. A revised ridge classification scheme is shown by the heavy black straight lines giving the spreading-rate ranges for ultraslow-, slow-, fast- and the two transitional classes. The SWIR and the Knipovitch ridge are examples of ultraslow- to slow-spreading transitional ridges while the intermediate-rate Southeast Indian ridge is an example of a slow- to fast-spreading transitional ridge. Transitional ridges exhibit alternating sections with the morphology of the faster- and slower-spreading classes, rather than representing intermediate characteristics between them. Broken lines indicate the typical overlap of tectonic styles for each of the three principal classes of ocean ridge that give rise to the two transitional ridge classes.

are largely partially serpentinized peridotite. The trough walls consist of a series of large irregular or lenticular blocks with smooth low-angle scarps (14° to 20°) that are highly oblique to the spreading direction, exposing abundant mantle peridotite. Many of these scarps appear to be simple fault surfaces that form continuous ramps ~6 km long rising 1 to 2 km from the rift valley floor to the crest of the rift mountains on which old axial horst blocks were uplifted to form linear ridges parallel to the ridge trend.

We traced hundreds of small northeastern- and southwestern-facing linear scarps and asymmetric ridges in the 50-m contour bathymetry all along the oblique supersegment, though most are too small to be visible in Fig. 3. Almost all are oriented nearly orthogonal to the spreading direction. These are interpreted as inward- and outward-facing high-angle normal faults that are only 50–150 m high, except at the major magmatic centres. They contribute little to the trough relief, and cut the walls at an acute angle, giving them an unusual serrated appearance. These faults can run long distances across the trough floor, up the walls and into the rift mountains.

A second major volcanic segment, also oriented perpendicularly to the spreading direction, is located at 14° 41′ E on a southeastward kink in the oblique supersegment centred on a large cross-axis topographic high. This 40-km-long 'Narrowgate' segment closely resembles the magmatic segments along the orthogonal supersegment with staircase normal faulting and a deep axial rift (>2,500 m relief). There is a well-defined axial neo-volcanic ridge, large

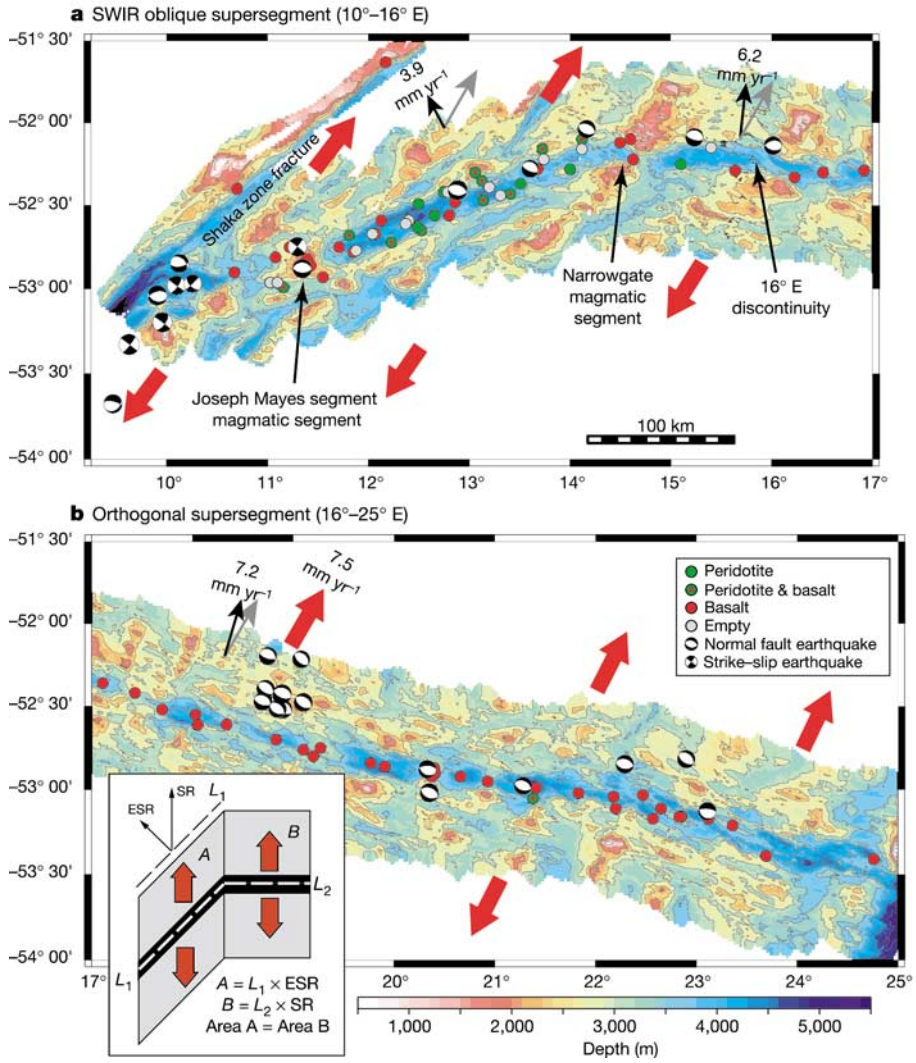

Figure 2 SWIR bathymetry from 9° to 25°E. We calculated spreading directions using fits to the SWIR transform from 2° to 37.5° E (red arrows). Fault solutions are for well-located Harvard catalogue earthquakes since 1977 of magnitude >4.5. Small circles give dredge locations and are larger than the tracks. **a**, Oblique supersegment mapped during RV *Knorr* cruise 162. **b**, Orthogonal supersegment mapped by ref. 25. The supersegment consists of ~42 ± 15 km en echelon second-order[16] magmatic ridge segments sub-perpendicular to the spreading direction. Their average magnetization anomaly is 15 A m^{-1} (ref. 25). Distinct circular MBA lows are centred about the western ridge segments, but to the east the signal is more chaotic[25]. This supersegment has a broader rift valley (~47 km) and greater cross-axis relief (~2.2 km), but closely resembles typical MAR spreading centres. In contrast to the oblique supersegment, rift mountain topography is broadly symmetrical north and south of the ridge, with local topographic highs and lows often matching on either side[25]. The inset in **b** illustrates the effect of ridge geometry on mantle upwelling. Where conductive heat loss becomes significant, the rate of mantle upwelling controls the extent of melting, lithospheric thickness and mantle rheology. Upwelling rate is a function of spreading rate (SR), ridge obliquity[13], and type of mantle flow (for example, buoyant three-dimensional versus passive two-dimensional)[50]. As a ridge becomes oblique to the spreading direction, its length increases per unit of lithosphere created, and mantle upwelling must slow proportionally to conserve mass. The 'effective spreading rate' for mantle upwelling (ESR), the spreading component orthogonal to the ridge trend, expresses these components. Black and grey arrows show the ESR and SR, respectively, at selected points along the ridge. Whereas the spreading rate here is nearly constant, the ESR is ~14.4 mm yr^{-1} at 18° E on the orthogonal supersegment, 12.4 mm yr^{-1} at the 16° E discontinuity and ~7.8 mm yr^{-1} at 12° E in the middle of the oblique supersegment (black arrows show half rates).

negative MBA and strong magnetization (Fig. 3). Pillow basalt was dredged from the neovolcanic zone[26], and basalt and diabase from the north wall.

From 14° 54′ E to the first orthogonal supersegment volcano at 15° 45′ E there is another oblique amagmatic accretionary segment with a deep axial trough. This trough curves gently east-southeast to connect the two supersegments. As this occurs, the ubiquitous high-angle normal faults gradually change from cutting across the axial trough, contributing little to the terrain, to become the principal terrain-forming element. One wall dredge recovered serpentinized peridotite, while another had scoria fragments thought to be glacial erratics.

The bathymetric and lithologic discontinuities are matched by geophysical ones as well, with an abrupt increase in MBA and

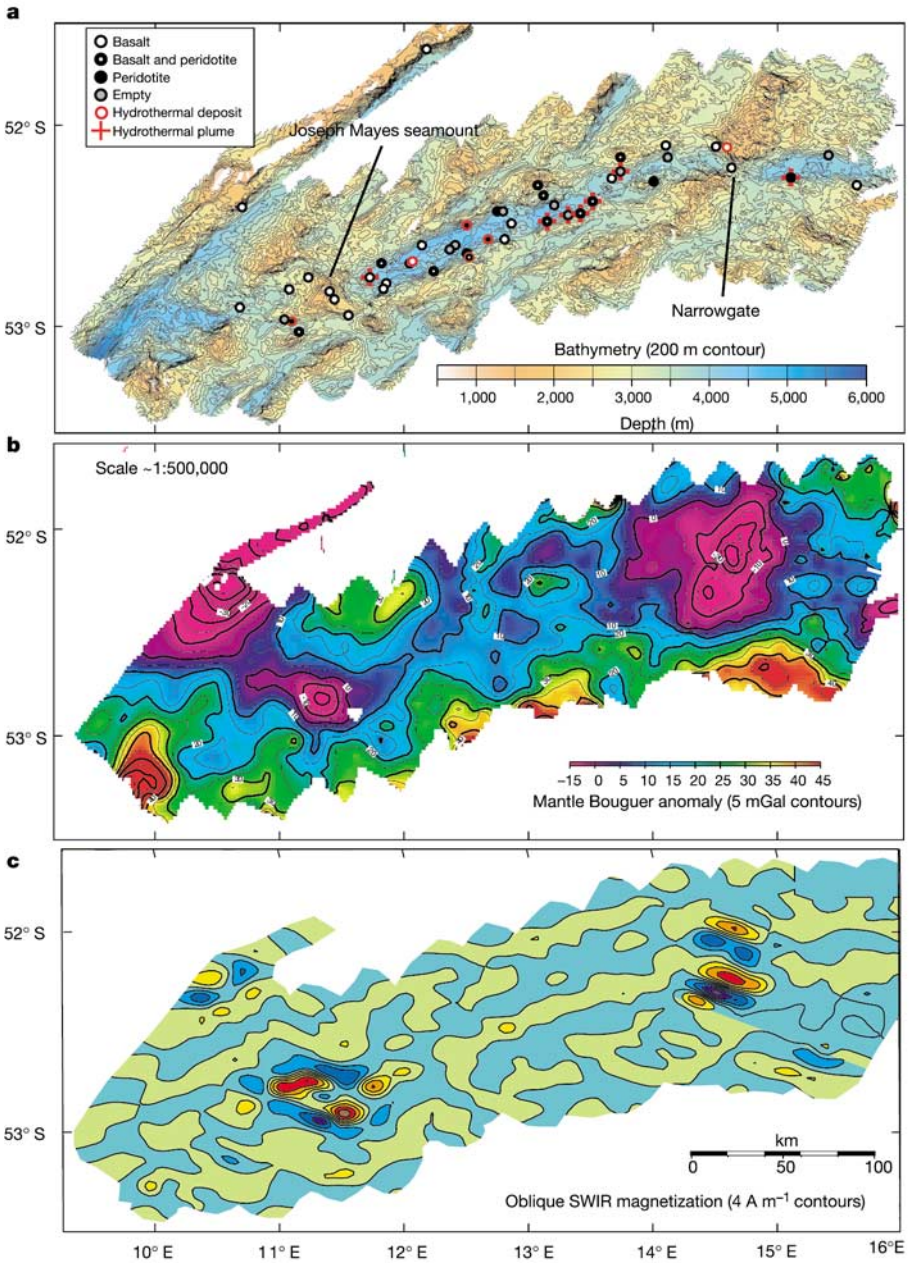

Figure 3 SWIR oblique supersegment bathymetric, mantle Bouguer and magnetization maps. **a**, 200-m contoured gridded bathymetry. **b**, Mantle Bouguer gravity anomaly. **c**, Crustal magnetization as the product of a nonlinear inversion that removed the topographic effect and the distortion resulting from the non-vertical magnetization and the Earth's magnetic field. Unlike the orthogonal supersegment, rift mountain topography is broadly asymmetric north and south of the ridge, with local topographic highs and lows rarely matching on crust of the same age on either side[25]. A small-diameter large-magnitude MBA low is centred at Joseph Mayes seamount, which is consistent with a recently formed volcanic segment splitting an older mantle block. The other large MBA low centred at Narrowgate extends into the rift mountains along the cross-axis topographic high, consistent with a thick belt of crust formed at a long-lived magmatic segment. At the eastern end of our survey is the edge of the previously recognized large MBA low over the first orthogonal supersegment magmatic segment[25] (**b**). This MBA low is similar in width but smaller in amplitude than the Narrowgate anomaly (20–25 mGal versus 35–40 mGal). 27 magnetic profiles were collected across the oblique supersegment out to about anomaly 5 (10 Myr ago). Only a few have anomalies resembling forward models of a symmetric geomagnetic reversal sequence, mostly centred near the Narrowgate cross-axis volcanic high. The best estimates of spreading rate are from lines over the Narrowgate segment and just east of the Shaka fracture zone. These give symmetric anomaly 2A full spreading rates of 14 mm yr^{-1} and 15 mm yr^{-1}, respectively. Note that the unusual sigmoidal shape of Joseph Mayes seamount appears to be due to fissure eruptions from the peaks that created volcanic ridges extending sub-perpendicular to the spreading direction to the west and east respectively.

decrease in crustal magnetization west of 16° E. West of 16° E there are only two prominent circular MBA lows, each centred over a volcanic centre. The low over Narrowgate extends out over the northeast-southwest cross-axis topographic high, consistent with a belt of thick crust (Fig. 3b). The MBA lows correspond to crustal magnetization highs similar to those at MAR magmatic ridge segments, with magnetization ranging from -15 to $+15\,A\,m^{-1}$ (Fig. 3c). By contrast, the oblique axial troughs have high MBAs, and low magnetization with weak linear axial anomalies, indicating thin or missing crust. Teleseismic earthquakes give orthogonal normal fault solutions, except for a strike-slip solution at Mayes seamount that may be related to rotations accompanying splitting of the peridotite block (Fig. 2). The ubiquitous high-angle normal faults are probable sources for the remaining earthquakes.

The oblique supersegment rift mountains, unlike the orthogonal supersegment, are highly asymmetric across the rift and very rough. They have regions of lenticular blocks elongated parallel to the ridge trend and oblique to the spreading direction, as well as contrasting regions with elevated, irregularly shaped plateaus and seamounts with a lineated fabric sub-perpendicular to the spreading direction. The lenticular blocks have moderate to strongly positive MBAs similar to those of the mantle blocks on the axial trough walls. The plateaus and seamounts have weak negative MBA and morphologically appear volcanic, dominating the northern and large portions of the southern rift mountains (Fig. 3b). There is also an abandoned fracture zone trace at 13.7° E. This and eastward V-shaped topographic trends in the rift mountains centred on Narrowgate and the 16° E magmatic segment suggest that the oblique amagmatic accretionary segments formed by the eastward migration of these magmatic ridge segments, and the gradual disappearance of others. Before ~8 Myr ago, then, this section of the SWIR seems to have consisted of magmatic ridge segments linked by transforms.

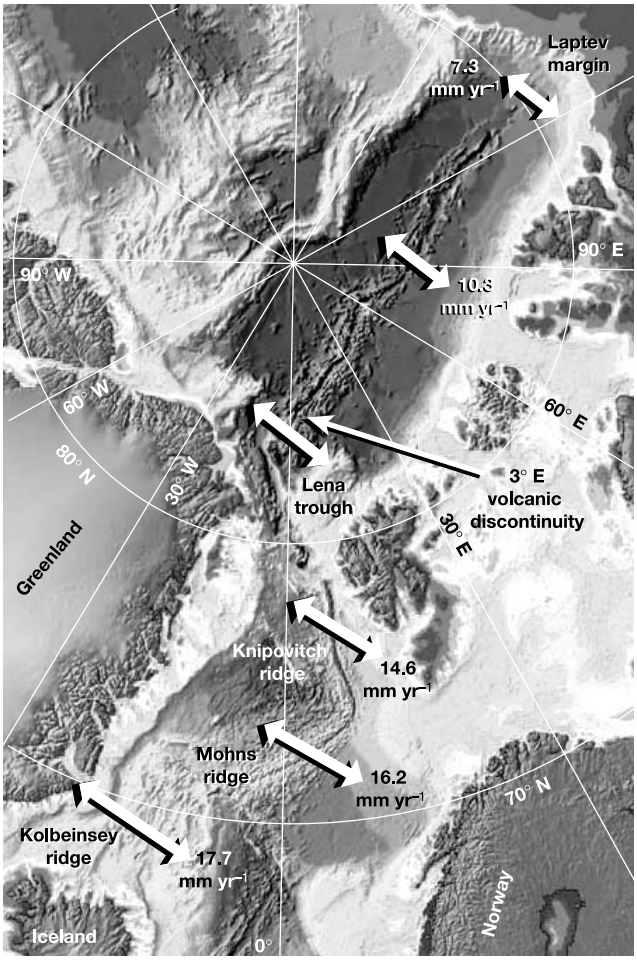

Figure 4 Arctic ridge system modified from the IBCAO bathymetry[51] showing its subdivisions including the Gakkel ridge and the Knipovitch ridge (see text). Also shown for reference is the position of the 3° E volcanic discontinuity. Spreading rates and azimuths are calculated from the Nuvel 1 model[27].

The Arctic ridge system

The Arctic ridge system (Fig. 4) from Iceland to 3° E on the Gakkel ridge is a transitional ridge like the SWIR, with spreading rate decreasing northward from $18\,mm\,yr^{-1}$ to $12.7\,mm\,yr^{-1}$ (refs 27, 28). It consists of long sections, each with their own name and character, that alternate between ultraslow- and slow-spreading physiography. In particular, the Knipovitch ridge is a ~550-km-long supersegment trending 41° to 55° from the spreading direction. The average ESRs of 11.2 and $12.3\,mm\,yr^{-1}$ in the north and south, respectively, fall at or below the ultraslow-spreading ESR threshold at 16° E on the SWIR. This supersegment contains no transforms and has all the physiographic features of the SWIR 10°–16° E oblique supersegment, including point-source volcanic centres and cross-axis bathymetric highs with MBA lows oriented perpendicularly to the spreading direction, linked by long deep oblique segments[29]. Heavy sedimentation, however, obscures many features, particularly between the volcanic centres, and limited dredging largely to the highs, which, like those at the SWIR oblique supersegment, yielded largely basalt.

Gakkel ridge, although it is the slowest-spreading ocean ridge, has no transform faults anywhere along its length[15,30]. Its spreading rate varies smoothly eastward as it nears its Euler pole from $12.7\,mm\,yr^{-1}$ to $6.0\,mm\,yr^{-1}$. With a near-orthogonal trend, the ESR equals the absolute spreading rate along most of it. The Gakkel ridge's trend conforms to the shape of the conjugate Lomonosov ridge and the Barents shelf margins, so, unlike the SWIR, its geometry is inherited from early continental rifting[15,31]. The 220-km-long faster section west of 3° E, like the SWIR from 16° to 25° E, consists of a string of magmatic ridge segments[32] lying in a deep rift valley bounded by high-angle normal faults. Abundant pillow basalt was dredged there[32], though relatively small magnetic anomalies and seismic measurements indicate a thin crust (~2–3 km)[10,33–35]. At 3° E, at a small non-transform offset, the rift valley floor drops 1 km, and only peridotite was dredged for 80 km to the east[32,36]. Scattered volcanics and peridotites then dominate to 13° E, where the first of a series of isolated magmatic segments occurs. These increase in number to 72° E, with mantle peridotite occurring rarely east of 40° E (ref. 32). East of 72° E volcanism may again diminish, as the rift is heavily sedimented and only two additional magmatic segments have been identified at 84° E and 92° E (ref. 37), while gravity measurements at 95° E suggest the crust is vanishingly thin there[38].

Bathymetry[15,23,32], magnetics[23,31,39], and sidescans[15,37] confirm the highly localized volcanism east of 3° E. This takes three forms: (1) volcanic segments centred on large cross-axis ridge-perpendicular highs, (2) large point-source volcanoes, and (3) large highly reflective flows locally ponded on the rift valley floor near major volcanic centres[15]. The ponded flows are probably thin, given their low magnetization[23,39]. Similar to the SWIR Narrowgate segment, the magnetization increases sharply at cross-axis volcanic highs and local axial highs[31], and rift valley wall morphology indicates large tectonic uplifts on high-angle normal faults. The rift valley floors shoal ~2 km to the midpoints of the magmatic segments, which are centred on prominent local MBA lows.

Between the volcanic centres are long deep rift valleys (~4,600–5,400 m) with weakly negative to slightly positive MBA[15] and low magnetic intensity[13,31]. Here the rift walls consist of long linear ridges or more irregular massive block uplifts exposing abundant peridotites[15,36] identical to faults bounding the 9°–16° E SWIR

amagmatic segments. They are 10–15 km across and 1–2 km high, with single low-angle scarps dipping 10° to 20° from the crest of the rift mountains to the valley floor[15,32]. Although most of the magmatic and amagmatic segments are orthogonal to the spreading direction, there is a 350-km section between 35° and 77° E where the ridge bends sharply to the north and back again, before resuming an orthogonal trend. Around the bend, magmatic segments remain oriented perpendicularly to the spreading direction, while amagmatic segments follow the ridge trend as at the SWIR oblique supersegment.

Discussion

The traditional division of ocean ridges is inadequate to characterize their full variability. Examples of ridges spreading less than $\sim$20 mm yr^{-1} show a common set of unusual tectonic features sufficient to characterize a new class of spreading ridges. Ultraslow-spreading ridges consist of linked magmatic and amagmatic accretionary segments, lack transform faults, and have discontinuous volcanism with large regions of highly attenuated or missing crust. Where the ESR varies continuously at the Gakkel ridge and the SWIR there are discontinuities at 12.4 and 12.0 mm yr^{-1} where magmatism stops abruptly, and the ridges shift from slow-spreading to ultraslow-spreading behaviour. Elsewhere on the SWIR and Arctic ridge system, we find ultraslow-spreading characteristics appearing when the ESR is less than $\sim$12 mm yr^{-1}. Thus, we pick 12 mm yr^{-1} absolute spreading rate as the usual boundary for ultraslow-spreading ridges, noting that changes in ridge geometry and mantle temperature and composition can cause ultraslow-spreading tectonics up to about 20 mm yr^{-1}.

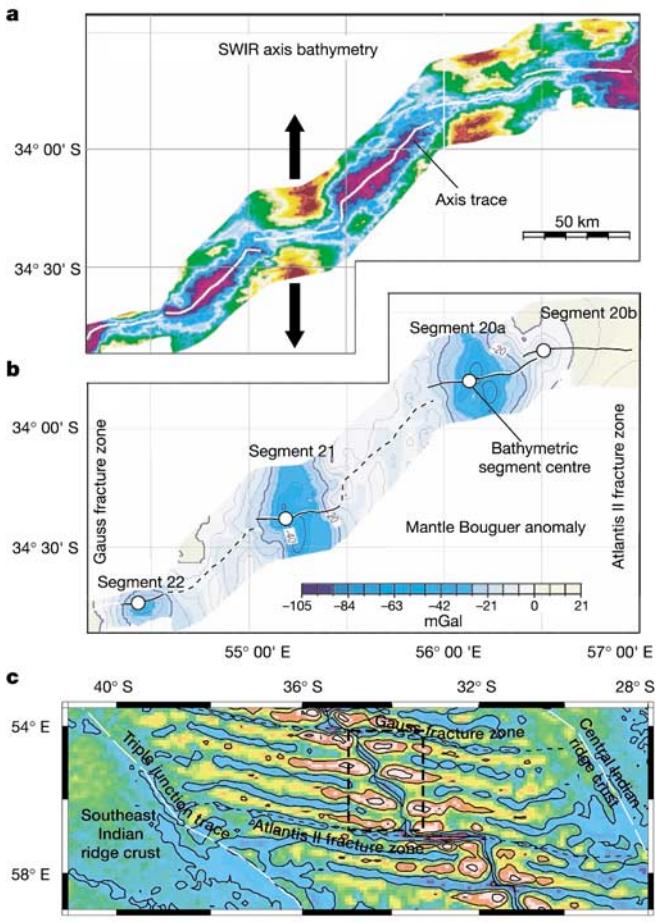

Figure 5 SWIR axial region between the Atlantis II and Gauss fracture zones (modified from ref. 24). **a**, Bathymetric map of the ridge axis showing greatest depths in blues and purples and shallowest in reds and yellows. Total depth range is from 6,500 to 1,850 m. **b**, Mantle Bouguer gravity anomaly map with 5-mGal contours. Trace of magmatic segments shown as thin black lines; trace of oblique amagmatic accretionary segments shown as dotted lines. **c**, Satellite free-air gravity map showing the location of the map areas in **a** and **b** (dashed box) and the traces of the oblique amagmatic accretionary segments across the Indian Ocean floor extending to the trace of the Rodriguez triple junction. These traces (thick dashed white line) separate the SWIR from the central and Southeast Indian ridge crust that formed as the triple junction migrated to the northeast with time. Spreading directions run parallel to the adjacent Atlantis II and Gauss transforms as indicated by the thick dotted lines.

A geochemical discontinuity matches the physiographic and crustal changes as well. Axial basalts on the faster-spreading side are generally typical MORB, and have lower Na_8 and higher Fe_8, while those on the slower side may be alkaline and/or isotopically enriched with high LREE and other incompatible trace-element abundances[26,32,40]. Na_8 and Fe_8 are the weight% Na_2O and FeO corrected for fractionation to 8 wt% MgO. High Na_8 may reflect large degrees of mantle melting, whereas high Fe_8 may reflect deep mantle melting[41]. This is consistent with dramatically lower extents of mantle melting beneath ultraslow ridges. Simple conductive models for variations in mantle melting with spreading rate do not predict a volcanic discontinuity of $\sim$12 mm yr^{-1} (refs 9, 11). This implies a threshold behaviour in mantle dynamics and melt generation, perhaps representing a switch from regions of continuous volcanism dominated by buoyant flow to regions dominated by passive flow.

Volcanism along ultraslow ridges, however, does not correlate with ESR. Long-lived volcanic centres tend to occur at bends at both the Gakkel ridge and the SWIR, suggesting a physical control on where melting occurs. The spatial distribution of mantle chemical heterogeneities also probably affects volcanism. Mayes seamount, for example, lies some 300 km west of the SWIR 16° E discontinuity and is possibly the largest non-hotspot-related axial volcano on the global ridge system. This may be explained by melting of a heterogeneous veined mantle. The isotopic composition of basalts and peridotites from the SWIR oblique supersegment are consistent with low degrees of melting of a veined mantle[42], while basalts erupted east of the 16° E discontinuity on the orthogonal supersegment are consistent with higher-degree melts dominated by a depleted host mantle peridotite[43]. Pyroxenite with a mid-ocean-ridge basalt (MORB)-like composition melts 35 to 50 km deeper than peridotite, and can be 60% molten at the peridotite solidus[44]. Thus when thermal conduction is sufficient to inhibit significant peridotite melting, there would still be vein melts that could aggregate and trigger local mantle diapirism. Excess enriched vein-melts aggregated from a broader region than usual for ridge volcanism could explain the enriched isotopic and trace-element composition of many basalts erupted at ultraslow ridges. Volcanism, then, would largely be a function of regional mantle composition and temperature, rather than spreading rate.

The abrupt shift to normal fault dominated terrain and the reorientation of the axis of faulting to perpendicular to the spreading direction at the magmatic segments at oblique ultraslow-spreading ridges is consistent with plate failure in the brittle regime, and suggests a major change in mantle dynamics. Despite their atypical chemistry, ultraslow-spreading volcanic centres are often as large as, or larger than, those at slow-spreading ridges. This heightened melt production suggests that mantle flow beneath these magmatic centres may have a buoyant component, whereas there is largely plate-driven passive flow beneath the amagmatic segments. Buoyant flow dramatically reduces the effects of conductive heat loss and would produce a thinner weaker lithosphere. More melt would also weaken the shallow lithosphere, notably by injection of magma in dykes, forming weak fluid-filled cracks. Gabbroic dykes found in East Pacific Rise mantle at Hess Deep[45] show that such cracks could extend at least 6 or 7 km in depth.

Amagmatic segments are identified here as a previously unrecognized class of accretionary plate boundary structure. On the

Gakkel ridge most amagmatic segments are orthogonal to the spreading direction, showing that their formation is not a function of ridge obliquity. The absence of strike-slip earthquakes on the SWIR from 9° to 16° E confirms that these amagmatic segments are not an oblique form of transform. Although this supersegment formed recently, amagmatic accretionary segments can form long-term stable plate boundaries. Between 54° and 57° E on the SWIR, ref. 24 describes oblique non-transform discontinuities, 50 and 76 km long, connecting three orthogonal segments (Fig. 5). The orthogonal segments are typical magmatic ridge segments with large-amplitude negative MBA lows. The central magnetic anomaly amplitudes, however, decrease from their midpoints towards the oblique segments. These oblique segments are not discontinuities, however, as they extend the ridge for 31 and 44 km respectively, perpendicularly to the spreading direction. They have ESR values of 10.8 and 10.6 mm yr^{-1}, lower relief and weak MBA lows. These, then, are amagmatic accretionary ridge segments. Satellite gravity maps[46] show depressed topography between the elevated magmatic segments extending in the spreading direction across the Indian Ocean to the triple junction trace, indicating that these linked magmatic and amagmatic segments formed a stable plate boundary for >50 Myr (Fig. 5c).

High-angle normal faults and fissures equivalent to the intra-rift faults seen at highly oblique slow-spreading ridges are abundant along the SWIR oblique supersegment. However, these cut the rift boundary faults rather than interacting with them as at slow-spreading ridges. At the same time, the rift boundary faults are very unlike those bounding faster-spreading ridges. This demonstrates that, unlike oblique slow-spreading ridges, these two fault sets form and operate independently. The highly unfavourable orientations for brittle failure of the major boundary faults at the oblique amagmatic segments imply that strain is localized by pre-existing structures formed outside the brittle deformation field. The primary mode of accretion along the amagmatic segments appears to be emplacement of mantle peridotite directly to the rift valley floor along the axis of rifting and parallel to the ridge trend, with subsequent fault capture and block rotation to form the rift valley walls. Because these structures are parallel to the ridge trend, we suggest that failure is localized by the axis of intrusion of the asthenosphere into the lithosphere along the zone of lithospheric necking at the base of the plate. This plate-driven horst and graben tectonics is similar to recent finite-element models for rifting of thick lithosphere at ridges[47], and may provide a new analogue to explain features of early continental rifting.

At the magmatic accretionary segments the principal faults and the axes of volcanic eruption are orthogonal to the spreading direction. These features are consistent with brittle extensional plate failure, and hence from the top of the plate. Thus a fundamental difference between magmatic and amagmatic accretionary segments is that the latter effectively represent failure initiated from the base of the plate, whereas the former represent failure largely initiated from the top. Why transforms disappear and a new class of accretionary plate boundary structure replaces them is unknown, although it does seem to be due to a thicker, colder and therefore stronger lithosphere.

Whereas fast-spreading ridges lack deep rift valleys, and their segmentation patterns evolve rapidly, reflecting thin lithosphere, slow-spreading ridge segmentation patterns evolve slowly, and their tectonics reflect the interplay of brittle deformation processes at the top of the plate associated with continuous volcanism and the forces arising from extension of a thicker lithosphere. At ultraslow-spreading ridges, however, these latter forces dominate the tectonics, except where a local magmatic segment forms. Thus slow-spreading ridge tectonics is intermediate between that at fast- and ultraslow-spreading ridges. There are thus three distinct classes of ocean ridge: fast-, slow- and ultraslow-spreading, with two transitional intermediate classes, because ridge tectonics are not simply a function of spreading rate, but also of ridge geometry, mantle composition and thermal structure. □

Received 23 December 2002; accepted 10 October 2003; doi:10.1038/nature02128.

1. Solomon, S. in *Drilling the Oceanic Lower Crust and Mantle, JOI/USSAC Workshop Report* (ed. Dick, H. J. B.) 73–74 (Woods Hole Oceanographic Institution, Woods Hole, MA, 1989).
2. Small, C. in *Faulting and Magmatism at Mid-Ocean Ridges* (eds Buck, W., Delaney, P. T., Karson, J. A. & Lagabrielle, Y.) 1–26 (American Geophysical Union, Washington DC, 1998).
3. Macdonald, K. C. in *The Western North Atlantic Region* (eds Vogt, P. & Tucholke, B.) 51–68 (Geological Society of America, Boulder, CO, 1986).
4. Heezen, B. C. The rift in the ocean floor. *Sci. Am.* **203,** 99–106 (1960).
5. Fornari, D. J., Haymon, R. M., Perfit, M. R. & Edwards, M. H. Geological characteristics and evolution of the axial zone on fast spreading mid-ocean ridges: formation of an axial summit trough along the East Pacific Rise, 9°-10°N 1998. *J. Geophys. Res.* **103,** 9827–9855 (1998).
6. Small, C. & Sandwell, D. T. An abrupt change in ridge axis gravity with spreading rate. *J. Geophys. Res.* **94,** 17383–17317 (1989).
7. Cochran, J. R. Systematic variation of axial morphology along the Southeast Indian Ridge. *Eos* **260,** 88 (1991).
8. Phipps Morgan, J. & Chen, Y. Dependence of ridge-axis morphology on magma supply and spreading rate. *Nature* **364,** 706–708 (1993).
9. Reid, I. & Jackson, H. R. Oceanic spreading rate and crustal thickness. *Mar. Geophys. Res.* **5,** 165–172 (1981).
10. Jackson, H. R., Reid, I. & Falconer, R. K. H. Crustal structure near the Arctic mid-ocean ridge. *J. Geophys. Res.* **87,** 1773–1783 (1982).
11. Bown, J. W. & White, R. S. Variation with spreading rate of oceanic crustal thickness and geochemistry. *Earth Planet. Sci. Lett.* **121,** 435–439 (1994).
12. White, R. S., Minshull, T. A., Bickle, M. J. & Robinson, C. J. Melt generation at very slow-spreading oceanic ridges: constraints from geochemical and Geophysical data. *J. Petrol.* **42,** 1171–1196 (2001).
13. Dick, H. J. B., Georgen, J. E., le Roex, A. P., Lin, J. & Madsen, J. A. The influence of ridge geometry on mantle melting at an ultra-slow spreading ridge. *Eos* F919 (1998).
14. Georgen, J. E., Lin, J. & Dick, H. J. B. Evidence from gravity anomalies for interactions of the Marion and Bouvet hotspots with the Southwest Indian Ridge: effect of transform offsets. *Earth Planet. Sci. Lett.* **187,** 283–300 (2002).
15. Cochran, J. R., Kurras, G. J., Edwards, M. H. & Coakley, B. J. The Gakkel Ridge: Bathymetry, gravity anomalies and crustal accretion at extremely slow spreading rates. *J. Geophys. Res.* **2003,** doi:10/1029/2002JB001830 (2002).
16. Macdonald, K. C., Scheirer, D. S., Carbotte, S. & Fox, P. J. It's only topography: Parts 1 & 2. *GSA Today* **3,** 1–35 (1993).
17. Kuo, B.-Y. & Forsyth, D. W. Gravity anomalies of the ridge-transform system in the South Atlantic between 31 and 34.5°S: Upwelling centers and variations in crustal thickness. *Mar. Geophys. Res.* **10,** 205–232 (1988).
18. Lin, J. & Phipps Morgan, J. The spreading rate dependence of three-dimensional mid-ocean ridge gravity structure. *Geophys. Res. Lett.* **19,** 13–16 (1992).
19. Tolstoy, M., Harding, A. J. & Orcutt, J. A. Crustal thickness on the Mid-Atlantic Ridge: Bull's-eye gravity anomalies and focused accretion. *Science* **262,** 726–729 (1993).
20. Magde, L. S. & Sparks, D. W. Three-dimensional mantle upwelling, melt generation, and melt migration beneath segment slow spreading ridges. *J. Geophys. Res.* **102,** 20571–20583 (1997).
21. Dauteuil, O. & Brun, J. P. Oblique rifting in a slow spreading ridge. *Nature* **361,** 145–148 (1993).
22. Clay, K. R. & White, M. J. Analogue modelling of orthogonal and oblique rifting. *Mar. Petrol. Geol.* **12,** 137–151 (1995).
23. Jokat, W. *et al.* Geophysical evidence for reduced melt production on the Arctic ultraslow Gakkel mid-ocean ridge. *Nature* **423,** 962–965 (2003).
24. Sauter, D. *et al.* The Southwest Indian Ridge between 49°15′ E and 57°E: focused accretion and magma redistribution. *Earth Planet. Sci. Lett.* **192,** 303–317 (2001).
25. Grindlay, N. R., Madsen, J. A., Rommevaux-Jestin, C. & Sclater, J. A different pattern of ridge segmentation and mantle Bouguer gravity anomalies along the ultra-slow spreading Southwest Indian Ridge (15°30′ E to 25°E). *Earth Planet. Sci. Lett.* **161,** 243–253 (1998).
26. le Roex, A. P., Dick, H. J. B. & Watkins, R. T. Petrogenesis of anomalous K-enriched MORB from the Southwest Indian Ridge: 11°53′ E to 14°38′ E. *Contrib. Mineral. Petrol.* **110,** 253–268 (1992).
27. DeMets, C., Gordon, R. G., Argus, D. F. & Stein, S. Current plate motions. *Geophys. J. Int.* **101,** 425–478 (1990).
28. DeMets, C., Gordon, R. G., Argus, D. F. & Stein, S. Effect of recent revisions to the geomagnetic reversal time scale on estimates of current plate motions. *Geophys. Res. Lett.* **21,** 2191–2194 (1994).
29. Okino, K. *et al.* Preliminary analysis of the Knipovich Ridge segmentation: influence of focused magmatism and ridge obliquity on an ultraslow spreading system. *Earth Planet. Sci. Lett.* **202,** 279–288 (2002).
30. Cochran, J. R. & Coakley, B. J. Morphology and segmentation of the Gakkel Ridge, Arctic Ocean, from SCICEX data. *Eos* **79,** F854 (1998).
31. Brozena, J. M. *et al.* New aerogeophysical study of the Eurasia Basin and Lomonosov Ridge: Implications for basin development. *Geology* **31,** 825–828 (2003).
32. Michael, P. J. *et al.* Magmatic and amagmatic seafloor generation at the ultraslow-spreading Gakkel Ridge, Arctic Ocean. *Nature* **423,** 956–961 (2003).
33. Jackson, H. R. & Reid, I. Oceanic magnetic anomaly amplitudes: variation with sea-floor spreading rate and possible implications. *Earth Planet. Sci. Lett.* **63,** 368–378 (1983).
34. Feden, R. H., Vogt, P. R. & Fleming, H. S. Magnetic and bathymetric evidence for the "Yermak Hot Spot" northwest of Svalbard in the Arctic Basin. *Earth Planet. Sci. Lett.* **44,** 18–38 (1979).
35. Duckworth, G. L., Baggeroer, A. B. & Jackson, H. R. Crustal structure measurements near FRAMII in the Pole Abyssal Plain. *Tectonophysics* **89,** 172–215 (1982).
36. Michael, P. J. *et al.* The Arctic Mid-Ocean Ridge Expedition—AMORE 2001—Seafloor spreading at the top of the world. *Eos* **82,** F1097 (2001).
37. Edwards, M. H. *et al.* Evidence of recent volcanic activity on the ultraslow-spreading Gakkel ridge. *Nature* **409,** 808–812 (2001).
38. Coakley, B. J. & Cochran, J. R. Gravity evidence of very thin crust at the Gakkel Ridge (Arctic Ocean). *Earth Planet. Sci. Lett.* **162,** 81–95 (1998).

39. Vogt, P., Taylor, P. T., Kovacs, L. C. & Johnson, G. L. Detailed aeromagnetic investigation of the Arctic Basin. *J. Geophys. Res.* **84,** 1071–1089 (1989).
40. Standish, J., Dick, H., le Roex, A., Melson, W. & O'Hearn, T. Major and trace element geochemistry: Ultra-slow spreading SWIR (9°–25° E). *Eos* **83,** F1331 (2002).
41. Klein, E. M. & Langmuir, C. H. Global correlations of ocean ridge basalt chemistry with axial depth and crustal thickness. *J. Geophys. Res.* **92,** 8089–8115 (1987).
42. Salters, V. J. M. & Dick, H. J. B. Mineralogy of the mid-ocean-ridge basalt source from neodymium isotopic composition of abyssal peridotites. *Nature* **418,** 68–72 (2002).
43. Mahoney, J., Le Roex, A. P., Peng, Z., Fisher, R. L. & Natland, J. H. Southwestern limits of Indian Ocean ridge mantle and the origin of low $^{206}Pb/^{204}Pb$ mid-ocean ridge basalt: isotope systematics of the Central Southwest Indian Ridge (17°-50°E). *J. Geophys. Res.* **97,** 19771–19790 (1992).
44. Pertermann, M. & Hirschmann, M. M. Anhydrous partial melting experiments on MORB-like Éclogite: Phase relations, phase compositions and mineral-melt partitioning of major elements at 2–3 GPa. *J. Petrol.* **44,** 2173–2201 (2003).
45. Dick, H. J. B. & Natland, J. Late stage melt evolution and transport in the shallow mantle beneath the East Pacific Rise. In *Scientific Results* (eds Gillis, K., Mevel, C. & Allan, J.) 103–134 (Ocean Drilling Program, Texas A&M University, College Station, TX, 1996).
46. Sandwell, D. T. & Smith, W. H. F. Marine gravity anomaly from Geosat and ERS 1 satellite altimetry. *J. Geophys. Res.* **102,** 10039–10054 (1997).
47. Poliakov, A. N. B. & Buck W. R. in *Faulting and Magmatism at Mid-Ocean Ridges* (eds Buck, W. R., Delaney, P. T., Karson, J. A. & Lagabrielle, Y.) 305–324 (American Geophysical Union, Washington DC, 1998).
48. Phipps Morgan, J., Parmentier, E. M. & Lin, J. Mechanisms for the origin of mid-ocean ridge axial topography; implications for the thermal and mechanical structure of accreting plate boundaries. *J. Geophys. Res.* **92,** 12823–12836 (1987).
49. Sotin, C. & Parmentier, E. M. Dynamical consequences of compositional and thermal density stratification beneath spreading centers. *Geophys. Res. Lett.* **16,** 368–377 (1989).
50. Forsyth, D. W. in *Mantle Flow and Melt Generation at Mid-Ocean Ridges* (eds Phipps Morgan, J., Blackman, D. K. & Sinton, J. M.) 1–66 (American Geophysical Union, Washington DC, 1992).
51. Macnab, R. & Jakobsson, M. The International bathymetric chart of the Arctic Ocean (IBCAO): An improved morphological framework for oceanographic investigations. *Geophys. Res. Abstr.* **5,** 10909 (2003).

Acknowledgements The National Science Foundation funded this work. We thank the crew and scientific party of RV *Knorr* Voyage 162, Legs 7-9 and the AMORE scientific party for discussions, particularly P. Michael, G. Kurras, C. Langmuir, J. Snow and W. Jokat. We also wish to acknowledge J. Standish for coordinating rock description on both cruises. J. P. Morgan, R. Buck, G. Hirth and J. Standish provided reviews of the manuscript, and R. Searle, and J. Cann provided us with additional insights into ridge tectonics.

Competing interests statement The authors declare that they have no competing financial interests.

Correspondence and requests for materials should be addressed to H.J.B.D. (hdick@whoi.edu).